Cuspidine-Like Compounds $Ln_4[Ga_{2(1-x)}Ge_{2x}O_{7+x}\square_{1-x}]O_2$ (Ln = La, Nd, Gd; $x \leq 0.4$)

Anthony Chesnaud, Olivier Joubert, Maria Teresa Caldes, Samrat Ghosh, Yves Piffard,* and Luc Brohan

Institut des Matériaux Jean Rouxel, UMR CNRS, Université de Nantes no. 6502 2, rue de la Houssinière, BP 32229-44322 Nantes Cedex 3, France

Received July 6, 2004. Revised Manuscript Received September 14, 2004

The $Ln_4[Ga_{2(1-x)}Ge_{2x}O_{7+x}\square_{1-x}]O_2$ (Ln = La, Nd, Gd; $x \leq 0.4$) compounds have been prepared first by solid-state reaction and then by a new regenerative sol−gel method which allows their sintering. They exhibit a Cuspidine-like structure. Upon substituting Ge^{4+} for Ga^{3+}, the Cuspidine structure is maintained up to $x = 0.4$. For $x \geq 0.15$ a 1D modulation of the structure was observed and analyzed as driven by composition. The Ge^{4+} substitution for Ga^{3+} with concomitant filling of oxygen vacancies is beneficial to the anionic conductivity which increases rather regularly with x to reach 10^{-3} S/cm at 800 °C for $x = 0.4$ and Ln = Nd. Conductivity measurements on $Ln_4[Ga_{2(1-x)}Ge_{2x}O_{7+x}\square_{1-x}]O_2$ (Ln = La, Nd, Gd) compounds with a fixed Ge content ($x = 0.2$) show a clear increase of the activation energy when the ionic radii of the Ln^{3+} cation decreases. La and Nd compounds exhibit similar conductivities, significantly larger than that of the Gd counterpart.

1. Introduction

Over the last three decades, solid oxide fuel cells have been attracting considerable interest because of the prospect of utilizing their high efficiency and environmentally friendly nature. However, the development of new materials with improved properties is still necessary before the introduction of fuel cells into widespread use will become a reality. In the present systems, the most widely used electrolyte is yttria stabilized zirconia (YSZ), but its high operational temperature (≥800 °C) induces severe restrictions upon the materials that can be used reliably and causes problems of lifetime. Therefore, there is a need for new oxide ion conductors with improved properties.

As part of these efforts to find suitable alternate electrolyte materials, we have recently initiated an evaluation of the potentialities of cuspidine-like compounds, and a preliminary investigation of the structural and transport properties of $Nd_4[Ga_{2(1-x)}M_{2x}O_{7+x}\square_{1-x}]O_2$ (M = Ti, Ge) compounds was reported.[1]

Minerals in the Cuspidine group are described by the formula $M_4(Si_2O_7)(O,OH,F)_2$, where M stands for cations in octahedral (or roughly octahedral) coordination.[2] The structure of the prototype Cuspidine compound, $Ca_4(Si_2O_7)(OH,F)_2$,[3] (space group (SG) $P2_1/a$ with $a = 10.906$ Å, $b = 10.521$ Å, $c = 7.518$ Å, and $\beta = 109.3°$) is built up from ribbons of edge sharing $Ca(O,OH,F)_6$ octahedra running parallel to the c axis, and Si_2O_7 groups (Figure 1). Such ribbons are interconnected by corner sharing

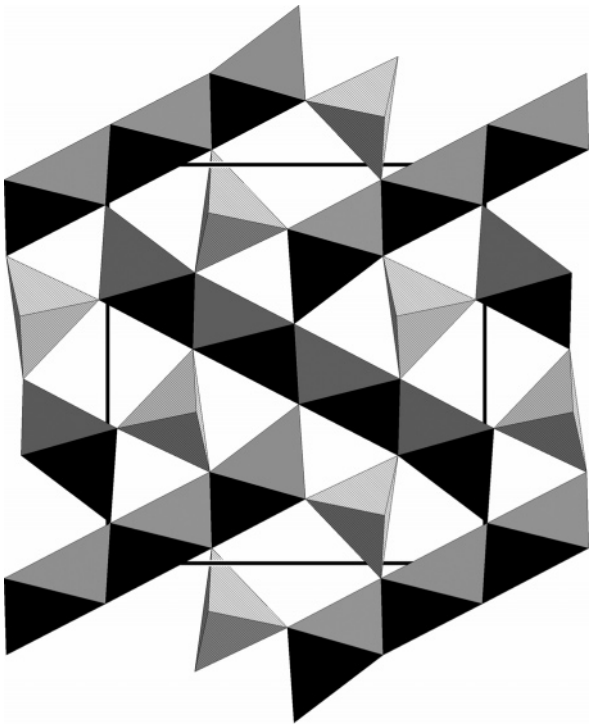

Figure 1. [100] View of the Cuspidine structure ($Ca_4(Si_2O_7)(OH,F)_2$) showing ribbons of edge sharing $Ca(OH,F)_6$ octahedra and SiO_4 tetrahedra (hatched).

to create an "octahedral" framework to which Si_2O_7 groups are linked via vertexes. Within the columnar arrangement of Si_2O_7 groups along the c axis, the intergroup Si−Si distance is ∼4.3 Å, and the empty site between can be considered as an anion vacancy. Therefore, the Cuspidine structure can also be viewed as an M_4X_8 (X = O, OH, F) "octahedral" framework delimiting channels wherein $(Si-O-Si\ \square)_n$ infinite chains are

* To whom correspondence should be addressed. E-mail: piffard@cnrs-imn.fr.

(1) Joubert, O.; Magrez, A.; Chesnaud, A.; Caldes, M.-T.; Jayaraman, V.; Piffard, Y.; Brohan, L. *Solid State Sci.* **2002**, *4*, 1413.
(2) Merlino, S.; Perchiazzi, N. *Can. Mineral.* **1988**, *26*, 933.
(3) Saburi, S.; Kawahara, A.; Henmi, C.; Kusachi, I.; Kihara, K. *Mineral. J.* **1977**, *8*, 286.

10.1021/cm048910t CCC: $27.50
Published on Web 11/12/2004

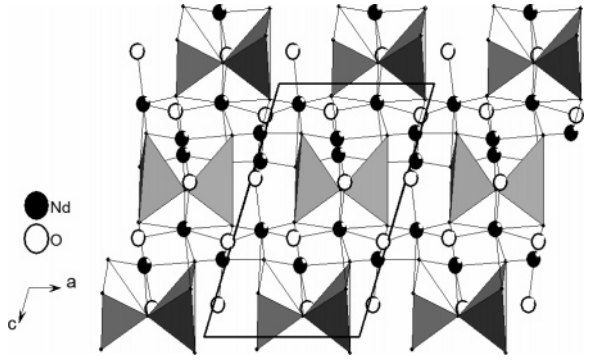

Figure 2. [010] View of a fragment of the $Nd_4(Ga_2O_7\square)O_2$ structure showing chains of Ga_2O_7 groups, Nd atoms and O atoms bonded to Nd only.

running parallel to the *c* axis [2], and its formula should better be written $Ca_4(Si_2O_7\square)(OH,F)_2$.

$Nd_4(Ga_2O_7\square)O_2$ is a group member of oxo-digallates with the Cuspidine structure[4] (Figure 2) and we have found that it offers possibilities of substitution at the gallium site.[1] However, although both Ti and Ge substitutions for Ga induce a concomitant filling of oxygen vacancies, opposite effects are observed on the oxide ion conductivity: Ti plays a detrimental role whereas the Ge improves the conductivity. A possible interpretation is that additional oxygen atoms are trapped in the coordination polyhedron of Ti^{4+} whereas they are forced to increase the coordination number of Ga^{3+}, i.e., to make a much weaker bond, when Ge^{4+} is introduced in the structure.

To learn more about the influence of Ge substitution on the microstructure of these interesting new oxide ion conductors, $Nd_4[Ga_{2(1-x)}Ge_{2x}O_{7+x}\square_{1-x}]O_2$ ($x \leq 0.4$) compounds have been investigated further by a combination of techniques including X-ray diffraction (XRD), selected area electron diffraction (SAED), and high-resolution electron microscopy (HREM). In addition, a new method has been developed which allows preparation of all materials in the form of dense pellets (with densities >95% of the theoretical) and therefore to perform more reliable electrical measurements. A comparison with previous data[1] is made. Finally, for a given Ge substitution rate, electrical measurements on the $Ln_4[Ga_{2(1-x)}Ge_{2x}O_{7+x}\square_{1-x}]O_2$ (Ln = La, Nd, Gd) compounds have been made to show the influence of the Ln^{3+} cation on the ion conductivity and activation energy (E_a).

2. Experimental Section

$Ln_4[Ga_{2(1-x)}Ge_{2x}O_{7+x}\square_{1-x}]O_2$ (Ln = La, Nd, Gd) compounds have been prepared first by solid-state reaction starting from Ln_2O_3, Ga_2O_3, and GeO_2. These reactants were ground thoroughly in acetone and heated to 1200 °C for 12 h. The resulting products were compacted in pellets, heated in air at 1400 °C for 48 h and cooled to room temperature (RT) by switching off the furnace. At this level, densities are about 80% of the theoretical, i.e., not enough for accurate measurements of the ionic conductivity. Therefore, a new method described below has been developed in order to obtain dense materials.

The sample morphology was studied using a JEOL JSM 6400F scanning electron microscope, and energy dispersive X-ray (EDX) analyses were systematically performed on numerous single crystals with a link system Oxford analyzer. Size distributions of particles (SDP) were measured with a Coulter LS230 instrument. XRD patterns of these materials were recorded at RT, using an Inel position sensitive detector (Cu $K\alpha_1$: $\lambda = 1.540598$ Å). Refinements of cell parameters were carried out using the program FULLPROF[5] and its interface: the program WinPLOTR.[6]

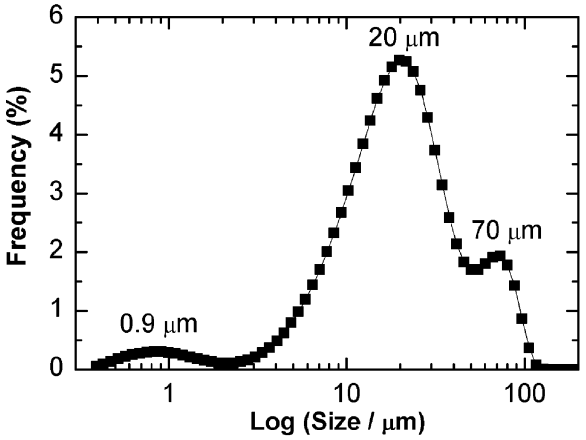

Figure 3. SDP of a sample of $Nd_4(Ga_2O_7\square)O_2$ prepared by solid-state reaction at 1200 °C for 12 h.

Thermal analyses were made on a Perkin-Elmer model TGS-2 TGA system. Surface area was measured on a Micromeretics ASAP 2010 instrument on samples dried at 100 °C for 5 h.

SAED studies were performed on a Philips CM30 electron microscope operating at 300 kV, and the HREM studies were carried out with a Hitachi H9000NAR electron microscope operating at 300 kV, with a Scherzer resolution of 1.8 Å. HREM image simulations were performed with the MacTempas[7] program using the multi-slice method.

Conductivity measurements were made with the use of samples in the form of pellets using model 1260 high-frequency response analyzer of M/s Solartron (Schlumberger, UK) between RT and 800 °C, in air. Both sides of the pellets were coated with a Pt paste to act as electrodes. Some measurements were also made under reduced oxygen partial pressures (10^{-5} atm using N_2 from the laboratory network, and 10^{-20} atm with an $Ar-H_2$ (5%) gas mixture) which were measured with the use of a YSZ oxygen sensor placed next to the pellet.

3. Results and Discussion

3.1. Investigation of Synthesis and Sintering Conditions. As already mentioned above, when materials were prepared by solid-state reaction, their sintering at 1400 °C did not lead to densities more than 80% of the theoretical, and this is probably a consequence of the broad distribution in grain size (Figure 3). Therefore, a sol−gel route has been developed starting from the material obtained by solid-state reaction at 1200 °C in order to avoid the use of other reactants which need to be soluble. As a matter of fact, if GeO_2 is not soluble in HNO_3, it is rather easy to effect solution of $Ln_4[Ga_{2(1-x)}Ge_{2x}O_{7+x}\square_{1-x}]O_2$ (Ln = La, Nd, Gd) compounds in this medium. This regenerative sol−gel method is a modified version of the nitrate polyacrylamide gel (NPG) process.[8]

(4) Schneider, S. J.; Roth, R. S.; Waring, J. L. *J. Res. Natl. Bur. Stand.* **1961**, *65A*, 345.

(5) Roisnel, T.; Rodriguez-Carjaval, J. FULLPROF. *Physica B* **1993**, *192*, 55. See also http://www-llb.cea.fr/fullweb/fp2k/fp2k.htm.

(6) Roisnel, T.; Rodríguez-Carvajal, J. WinPLOTR: a Windows Tool for Powder Diffraction Patterns Analysis. In *Materials Science Forum, Proceedings of the 7th European Powder Diffraction Conference (EPDIC 7)*; Trans. Tech. Publications Ltd.: Zurich-Uetikon Switzerland, 2000; Parts 1&2, pp 118−123. See also http://www-llb.cea.fr/fullweb/winplotr/winplotr.htm.

(7) Kilaas, R.; MacTempas, Total Resolution, Berkeley. See also http://www.totalresolution/Mactempas.html.

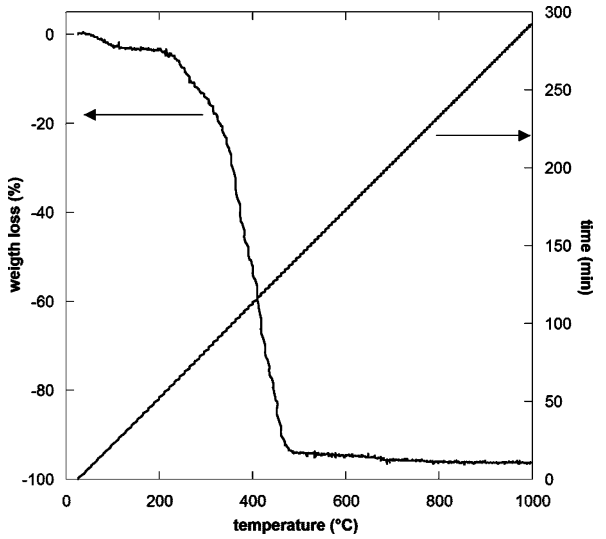

Figure 4. TG curve of the raw material (see Section 3.1) prepared by the NPG process and further heated for 20 min in a microwave oven (600 W).

About 300 mg (~0.35 mmol) of the starting material was dissolved within 5 min in 20 mL of 1.2 M HNO_3 at 80 °C. Cations complexation was achieved by adding to this solution 5 g of diammonium citrate (~22 mmol) which acts as a chelating agent. For the gelation process an organic monomer—10 mL of acrylic acid (AA)—and a reticulating agent—1 g of *N, N′*—methylene-bis-acrylamid (MBA) were added and dissolved into this solution. No turbidity or precipitate was observed at any stage of processing. At this level, a polymerization initiator affording free radicals, such as α,α′ azo-iso-butyronitrile, is usually added but this compound is highly toxic and explosive. Therefore, it was found convenient to replace it by H_2O_2 (30% in weight). Upon addition of one drop of H_2O_2 into the boiling solution a transparent gel was obtained almost instantaneously.

Water and part of the organic species were then removed by heating of the monolith gel for 20 min in a microwave oven (600 W). The resulting material is a dark-brown crisp resin which was crushed prior to charring and calcination. In the case of $Nd_4(Ga_2O_7\square)$-O_2, this raw material was subjected to a TG analysis. The TG curve displayed in Figure 4 shows that the weight loss, which is rather huge (~96%), occurs in several steps between RT and 470 °C, the most important being observed between 200 and 470 °C. Above 470 °C, the TG curve shows a plateau region which extends up to 1000 °C. Therefore, one can assume that at 470 °C all organic species are decomposed, leading to a pure oxide product whose composition remains fixed up to 1000 °C. To follow the crystallization process, samples of the raw material were calcined for 6 h at various temperatures ranging from 600 to 900 °C; after cooling to RT, the XRD patterns of the resulting products were recorded. They are displayed in Figure 5 which shows that the oxide material remains amorphous up to 600 °C. At 700 °C the powder pattern of $Nd_4(Ga_2O_7\square)O_2$ can be clearly identified. The powder obtained at 900 °C is made of agglomerates (Figure 6a) of fine grains (~50 to ~100 nm) (Figure 6b) and, as expected, the surface area

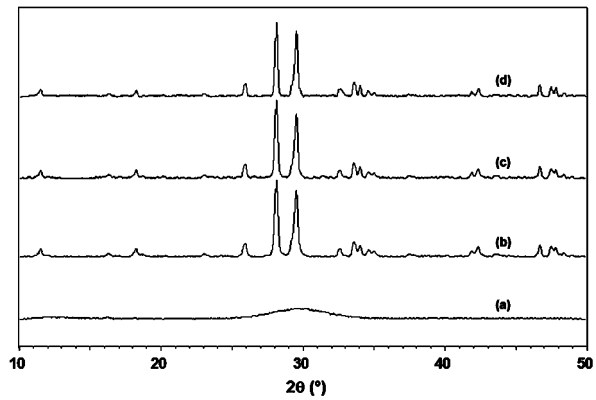

Figure 5. XRD patterns of materials obtained upon heating the raw material (the same as in Figure 3) in air for 6 h at *T*, and cooling to RT: (a) $T = 600$ °C, (b) $T = 700$ °C, (c) $T = 800$ °C, (d) $T = 900$ °C.

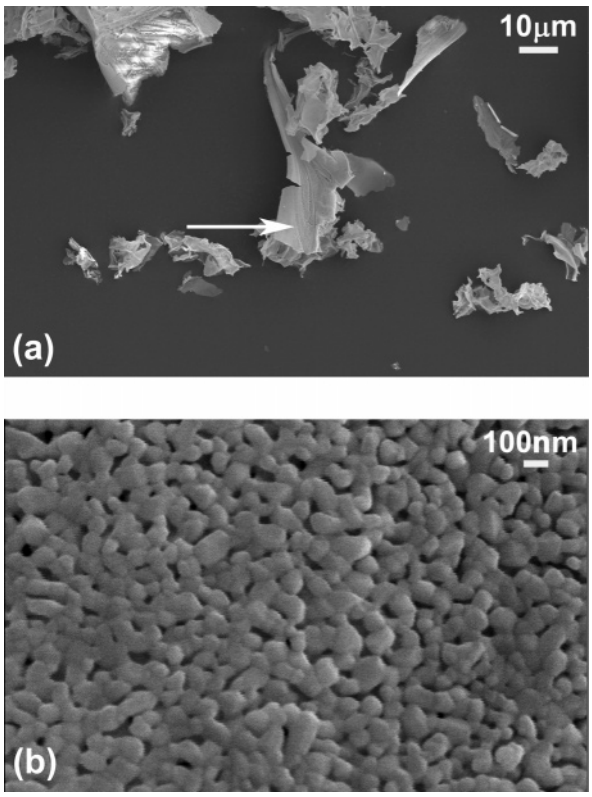

Figure 6. SEM micrographs of a sample of $Nd_4(Ga_2O_7\square)O_2$ prepared by sol−gel method and heated at 900 °C for 6 h: (a) agglomerates of small crystals, (b) enlarged image of a zone indicated by the arrowhead in (a).

Table 1. Evolution of the Surface Area of $Nd_4(Ga_2O_7\square)O_2$ Samples with the Preparation Conditions

preparation method	temperature (°C)	duration (h)	surface area ($m^2 \cdot g^{-1}$)
sol−gel	700	6	20.5(1)
sol−gel	800	6	9.8(1)
sol−gel	900	6	4.3(1)
solid state	1200/1400	24/48	0.4(1)

of materials prepared via this sol−gel route is much larger than that measured on a sample of $Nd_4(Ga_2O_7\square)$-O_2 prepared by solid-state reaction (Table 1). However, one can observe a clear decrease of the surface area when the calcination temperature increases.

After that, the preparation of dense pellets was undertaken. About 250 mg of the materials were first

(8) Douy, A.; Odier, P. *Mater. Res. Bull.* **1989**, *24*, 1119.

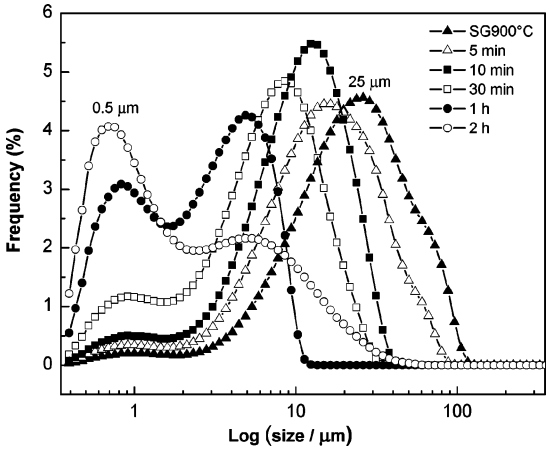

Figure 7. SDP (in volume) before (designated SG900 °C) and upon ultrasonic treatment of the $Nd_4(Ga_2O_7\square)O_2$ sample prepared by sol−gel method and heated at 900 °C for 6 h.

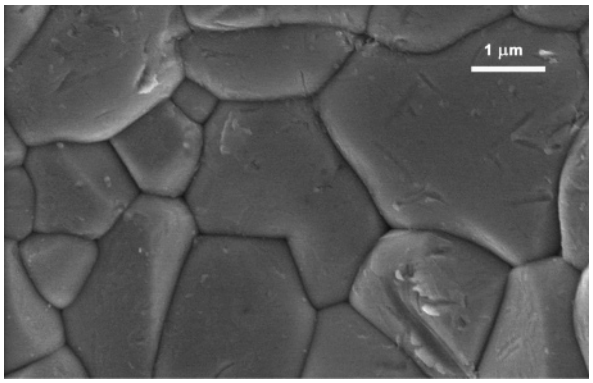

Figure 8. SEM micrograph of a fracture surface of a dense pellet of $Nd_4(Ga_2O_7\square)O_2$.

pressed in the form of disks with the use of an 8-mm die, under a uniaxial pressure of 250 MPa, and these green compacts were sintered in air at 1400 °C for 12 h. When the starting material is taken as such, i.e., nondeagglomerated material calcined at 900 °C, the sintering process is not very efficient and the final density is only ∼80%. A similar effect was already observed in the sintering process of $BaTiO_3$ elaborated by the citric process, and it was demonstrated that a partial deagglomeration was necessary prior to sintering.[9,10] In the present case this deagglomeration can be obtained by ultrasonic dispersion (Figure 7). With the use of these deagglomerated powders very dense ceramics were obtained (∼98% of the theoretical density). The microstructure of one of them, $Nd_4(Ga_2O_7\square)O_2$, appears in Figure 8 showing grains of 0.5−8 μm in size. All samples were further analyzed for their cation content by EDX on grains chosen on different areas. Such elemental analyses gave nominal formulas in very good agreement with starting compositions and were indicative of compositional homogeneity of samples upon sintering at high temperature.

3.2. Structural Studies. In our previous work,[1] SAED experiments were performed on $Nd_4[Ga_{2(1-x)}Ge_{2x}O_{7+x}\square_{1-x}]O_2$ compounds with $x = 0.05$, 0.1, and 0.15.

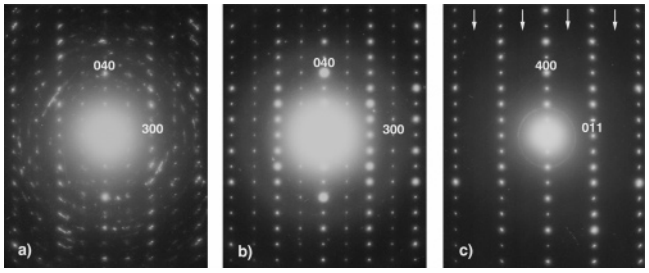

Figure 9. SAED patterns along the $[001]_m$ zone axis for (a) $x = 0.05$ and (b) $x = 0.1$, and along the $[01\bar{1}]_o$ zone axis for (c) $x = 0.15$.

Table 2. Cell Parameters of $Nd_4[Ga_{2(1-x)}Ge_{2x}O_{7+x}\square_{1-x}]O_2$ Compounds as a Function of x

x	a_m (Å)	b_m (Å)	c_m (Å)	β (deg)
0	7.7682(3)	10.9779(4)	11.4782(4)	109.04(2)
0.05	7.7733(3)	10.9636(4)	11.4894(4)	109.10(2)
0.10	7.7760(3)	10.9455(4)	11.5166(4)	109.34(2)
x	a'_m (Å)	b'_m (Å)	c'_m (Å)	β' (deg)
0.15	3.8890(2)	10.9318(4)	10.8821(4)	90.04(2)
0.20	3.8906(2)	10.9219(4)	10.8829(4)	90.05(2)
0.25	3.8949(2)	10.9144(4)	10.8764(4)	90.06(2)
0.30	3.9005(2)	10.9001(4)	10.8671(4)	90.06(2)
0.35	3.9007(2)	10.8849(4)	10.8602(4)	90.04(2)
0.40	3.9049(2)	10.8741(4)	10.8586(4)	90.01(2)

Table 3. Cell Parameters of $Ln_4[Ga_{1.6}Ge_{0.4}O_{7.2}\square_{0.8}]O_2$ Compounds (Ln = La, Nd, Gd)

Ln	a'_m (Å)	b'_m (Å)	c'_m (Å)	β' (deg)
La	4.0022(2)	11.1805(4)	10.9689(4)	90.182(3)
Nd	3.8906(2)	10.9219(4)	10.8829(4)	90.05(2)
Gd	3.7763(2)	10.6824(4)	10.8383(4)	90.071(3)

This study has shown that a monoclinic cell similar to that of $Nd_4(Ga_2O_7\square)O_2$ (SG $P2_1/c$) is maintained up to $x = 0.1$. For $x = 0.15$, $hk0$ reflections with odd h values are no longer observed on the $[001]_m$ SAED patterns (Figure 9), which suggests that the monoclinic a_m parameter is halved. At this substitution rate the structure can be described either in a "pseudo-orthorhombic" monoclinic cell (SG $P2_1/n$) with $a'_m \approx a_m/2$, $b'_m \approx b_m$, $c'_m \approx c_m \sin\beta\sqrt{1-(\tan\beta')^{-2}}$, and $(\tan\beta')^{-1} \approx (\tan\beta)^{-1} + a_m/2c_m \sin\beta$, or in the orthorhombic SG $Pnam$, with $a_o \approx b_m$, $b_o \approx c_m \sin\beta$, and $c_o \approx a_m/2$, because, upon refinement of the cell parameters from XRD patterns (Tables 2 and 3), it appears that the deviation of β' from 90° is so small that a convergent beam electron diffraction (CBED) study would be necessary to distinguish between monoclinic and orthorhombic symmetry.

On the $[010]_o$ SAED pattern of the $x = 0.15$ member (Figure 10a), some weak satellites were observed,[1] indicating an incommensurate modulation of the structure. To better analyze the structural modulation of these compounds, SAED studies have been undertaken on the $x = 0.3$ and 0.4 members and the previous electron diffraction study of the $x = 0.15$ member [1] has been completed. For all these compounds, the 3D reciprocal lattice was reconstructed from SAED tilt series and all main reflections were indexed using SG $Pnam$.

In Figure 10, the $[010]_o$ SAED patterns corresponding $x = 0.15$, 0.3, and 0.4 can be compared. While strong reflections in these patterns come from the average structure, the weak satellites observed in Figure 10a−c (an enlarged image is given in Figure 10d), between $h0l$

(9) Le Calvé-Proust, C.; Husson, E.; Odier, P.; Coutures, J.-P. *J. Eur. Ceram. Soc.* **1993**, *12*, 153.
(10) Miot, C.; Proust, C.; Husson, E. *J. Eur. Ceram. Soc.* **1995**, *15*, 1163.

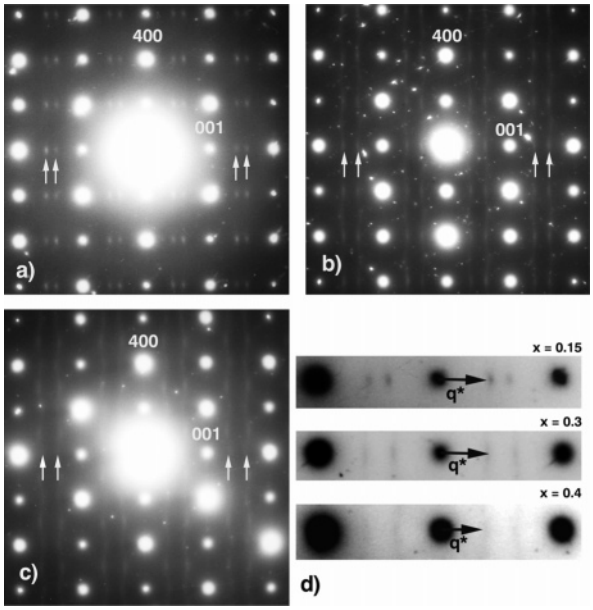

Figure 10. SAED patterns along the $[010]_o$ zone axis for (a) $x = 0.15$, (b) $x = 0.3$, and (c) $x = 0.4$. Positions along $[001]_o$* of the weak satellites are indicated by white arrows. (d) Enlarged image of the $[001]_o$* rows.

reflections along $[001]_o$*, result from a modulation of the average structure. For $x = 0.15$, though such satellites are slightly diffuse the modulation appears as mainly 1D. For $x = 0.3$ and 0.4, it can be seen (Figure 10b and c) that satellite reflections, though rather sharp along $[001]_o$*, extend as diffuse streaks along $[100]_o$* and that the intensity along these streaks is modulated. This indicates that for the largest Ge contents, besides modulation, a disorder appears in the (b_o,c_o) plane. Moreover in the case of $x = 0.4$, according to the position of intensity maxima along these streaks, it appears that the actual modulation is likely no longer 1D. Note that these satellites are still observed at 800 °C. If one takes into account the modulation along $[001]_o$*, the modulation vector is $q^* = \rho_{exp}\ c_o^*$ where ρ_{exp} decreases from ~0.45 to ~0.32 when x increases from 0.15 to 0.4.

At this level one can wonder why the solid solution is limited to $x = 0.4$, which kind of local order can induce this 1D modulation, and why the length of the modulation vector decreases continuously when x increases.

Upon substituting Ge^{4+} for Ga^{3+}, the concomitant filling of oxygen vacancies along c_o induces an increase in the average coordination number of cations within the columnar arrangement of $[M_2O_{7+x}\square_{1-x}]$ entities, i.e., every time an oxygen vacancy is filled, two of these cations must adopt the 5-fold coordination. However, since Ga^{3+} is obviously much more propitious to 5-fold coordination than Ge^{4+}, one can suppose that when two adjacent anionic sites are filled along c_o, the cation site between is preferentially occupied by Ga^{3+} as illustrated in Figure 11. This means that within the columnar arrangement of $[Ga_{2(1-x)}Ge_{2x}O_{7+x}\square_{1-x}]$ entities, $x/(1-x)$ of the Ga^{3+} cations adopt the 5-fold coordination, and that there are $(1-x)$ tetrahedral sites available for x Ge^{4+} cations. Therefore, for small x values, in addition to several local orders of O,□ sites, several local orders of the Ga,Ge atoms are possible along the c_o axis (Figure 11). When x increases the proportion of cationic sites exhibiting a 4-fold coordination, i.e., $(1-x)$, decreases

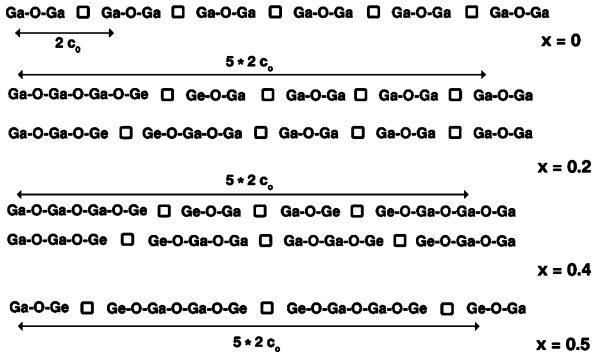

Figure 11. Schematic representations of possible distributions of both Ga,Ge and O,□ along the c_o axis (for $x = 0.2$ and 0.4 two distributions are shown).

rapidly. Consequently, the number of Ga/Ge distributions consistent with the nominal composition decreases drastically and $x = 0.5$ corresponds to the limit for which all Ga^{3+} cations would exhibit a 5-fold coordination and all tetrahedral sites would be occupied by Ge^{4+} cations, leading to only one possible distribution of Ga,Ge and O,□ along the c_o axis, i.e., to a complete segregation (ordering) of Ge^{4+} and Ga^{3+} cations. Our experiments have shown that it is not possible to reach this theoretical limit.

In $Nd_4(Ga_2O_7\square)O_2$, the Ga−Ga distance (3.45 Å) within a Ga_2O_7 group is significantly shorter than the inter-group distance (4.33 Å). Upon substituting Ge for Ga, oxygen atoms are introduced in the inter-group vacancy and Rietveld analyses have shown[1] that distances between such cations tend to equalize. However, for $x \leq 0.1$ they remain sufficiently different and weak $hk0$ reflections with odd h values are observed on the $[001]_m$ SAED patterns. This means that up to $x = 0.1$ local distortions introduced by the substitution of some Ge^{4+} for Ga^{3+} and concomitant filling of some oxygen vacancies do not affect significantly the ordered arrangement of Ga and O atoms (and oxygen vacancies) existing along the a_m axis of the structure of $Nd_4(Ga_2O_7\square)O_2$; its periodicity remains the same with however a clear decrease in the intensity of $hk0$ reflections with odd h values. For larger substitution rates ($x \geq 0.15$) the symmetry becomes orthorhombic with a periodicity $c_o \approx a_m/2$ and Rietveld analyses indicate that intra- and inter-group distances between cations of $[M_2O_{7+x}\square_{1-x}]$ entities are equal. However, this result corresponds to an average description of the actual structure which is modulated along the c_o axis. That a discrete modulation appears indicates both that distances between cations are not strictly identical, and, however, that there exists a uniform distribution of different spacings between cations (between oxygen atoms and between vacancies as well) which are multiples of c_o. From possible distributions of both Ga,Ge and O,□ corresponding to various x values, one can try to identify such spacings. This is done in Figure 12**,** where spacings have been taken as the various distances between consecutive oxygen atoms along the c_o axis. Starting from a sequence of n identical $2c_o$ spacings as in $Nd_4(Ga_2O_7\square)O_2$ (Figure 12a), upon filling a fraction x of □-sites, two types of new spacings are generated: "1" and "2" (in units c_o). When a fraction x of □-sites is filled, $2x$ spacings "1" are generated and x spacings "2" disappear. Therefore, the number of spacings within a

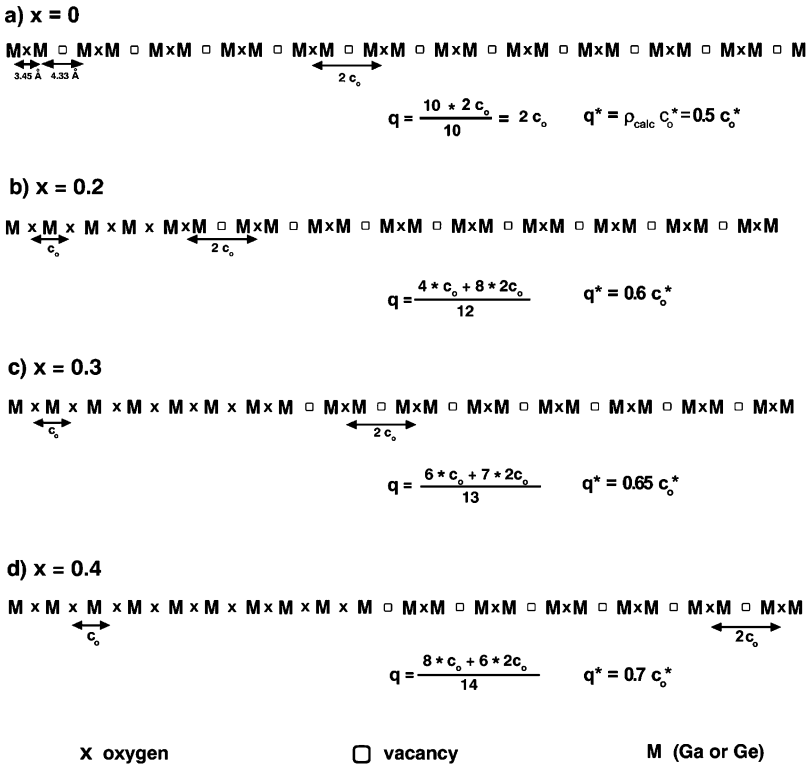

Figure 12. Schematic illustration of the 1D modulation along the c_o axis. "1" and "2" spacings (in units c_o) are indicated and examples of ρ_{calc} calculation are given.

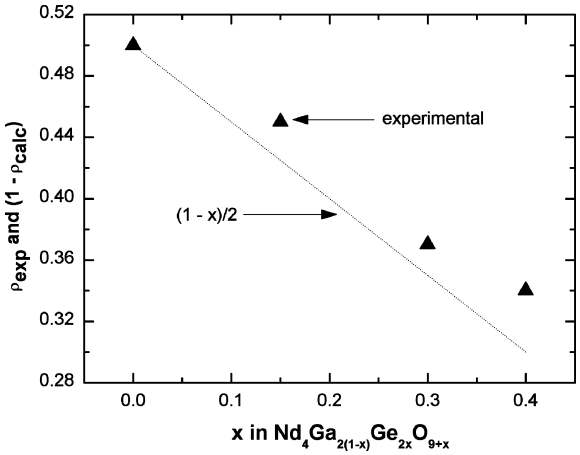

Figure 13. Evolution of ρ_{exp} and $(1 - \rho_{calc})$ with composition.

total length of $2nc_o$ increases, just like the number of oxygen atoms, from n to $(1 + x)n$. From sequences such as those displayed in Figure 12b–d, ρ_{calc} values can be determined according to a method described in ref 11. ρ_{calc} is simply the ratio between the number of spacings which characterizes a sequence and the total length of this sequence (in units c_o), i.e., $\rho_{calc} = (1 + x)n/2n = (1 + x)/2$. Therefore, according to this simple model, the 1D modulation appears as driven by composition only, and it can be seen (Figure 13) that it leads to ρ_{calc} values in fair agreement with experimental $(1 - \rho_{exp})$ values. This means that, in a first approach, this simplified model of 1D modulation agrees rather well with the position of satellite reflections along $[001]_o$*.

(11) Amelinckx, S.; Van Dyck, D. In *IUCr Monographs on Crystallography, Electron Diffraction Techniques*; Cowley, J. M., Ed.; 1995; Vol. II, ch. 4; Oxford Science Publications.

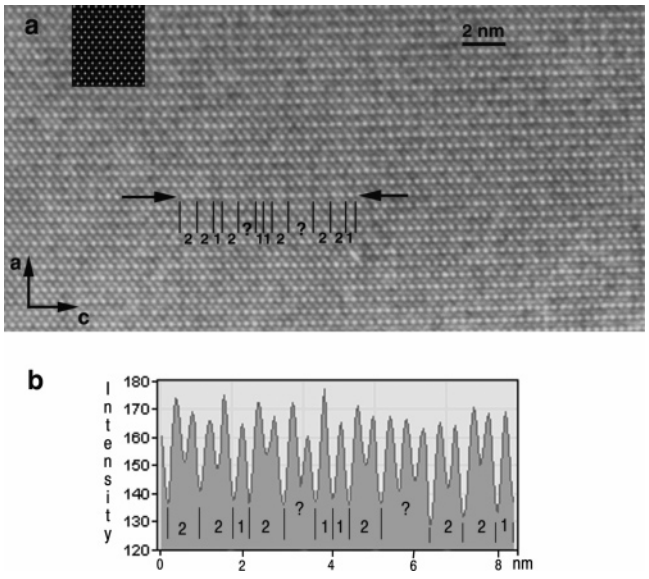

Figure 14. (a) Experimental $[010]_o$ HREM image corresponding to $x = 0.15$. The calculated contrast is included as an inset. (b) Experimental histogram imaging the modulation of intensity observed within the row of white dots delimited by black arrows on the experimental image.

At this level a HREM study was undertaken to appreciate the effect of the modulation on the experimental contrast and, if possible, to identify actual sequences. A characteristic $[010]_o$ HREM image, obtained for $x = 0.15$, is displayed in Figure 14a. The simulated contrast (displayed as an inset) was calculated (calculation parameters: defocus value −60 nm, thickness 7 nm) with the use of atomic positions inferred from the Rietveld study which does take the modulation into account. It must be mentioned that in this $[010]_o$

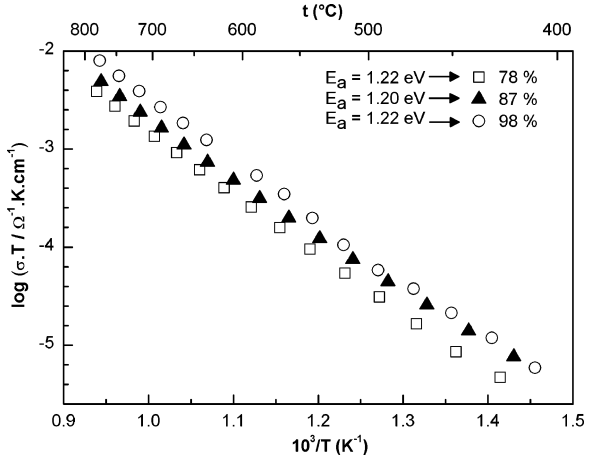

Figure 15. Conductivity data obtained for three pellets of $Nd_4(Ga_2O_7\square)O_2$ with densities ranging from 78 to 98% of the theoretical.

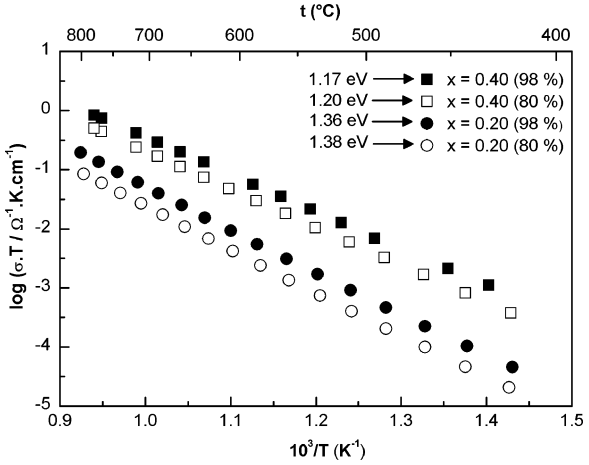

Figure 16. Arrhenius plots for $Nd_4[Ga_{2(1-x)}Ge_{2x}O_{7+x}\square_{1-x}]O_2$ ($x = 0.2$ and 0.4) samples prepared by solid-state reaction (density ~80%) and by sol−gel method (density ~98%).

projection all cations (including Nd^{3+}) are nearly superimposed and that, for this defocus value, they appear as white dots. Since this calculated contrast is based on an average description of the structure, it does not show any modulation of intensity within the rows of white dots. On the other hand the experimental contrast along such rows is modulated as illustrated by the histogram of Figure 14b which enables distinction of some "1" and "2" spacings (in units c_o); however, it is almost impossible to identify actual sequences. This is not surprising, because, due to the thickness of the sample (~7 nm), the contrast analysis is always made within a zone including several superimposed rows of $[M_2O_{7+x}\square_{1-x}]$ entities. Therefore, since for a given x value (i.e. for a single c_o value) there are many possible distributions of both Ga,Ge and O,□ along the c_o axis, the experimental contrast is always the addition of several sequences (not necessarily identical from one row to the other) leading to an averaging effect.

3.3. Conductivity Measurements. Conductivity measurements were made between RT and ~800 °C. In a first step the influence of density of sintered pellets on both the activation energy and ion conductivity was evaluated. Figure 15 shows the evolution of the conductivity of $Nd_4(Ga_2O_7\square)O_2$ vs temperature for three pellets with densities ranging from 78 to 98% of the theoretical. It can be seen that, as anticipated, the activation energy remains nearly the same. On the other hand the influence on the conductivity, though not drastic, is clearly visible: the larger the density the higher the conductivity which is multiplied by about two when the density increases from 78 to 98% of the theoretical. Similar effects can be observed in Figure 16 which enables one to compare Arrhenius plots for $Nd_4[Ga_{2(1-x)}Ge_{2x}O_{7+x}\square_{1-x}]O_2$ ($x = 0.2$ and 0.4) samples prepared by solid-state reaction (density ~80%) and by the sol gel method mentioned above (density ~98%). Therefore, in the case of Cuspidine-type compounds, the use of pellets with densities of only ~80% does not appear so critical for electrical measurements though it leads to slightly underestimated values of the ionic conductivity. However, one must keep in mind that the preparation of a dense material, strictly impermeable to gases, remains a requirement for its practical use as a solid electrolyte in a fuel cell.

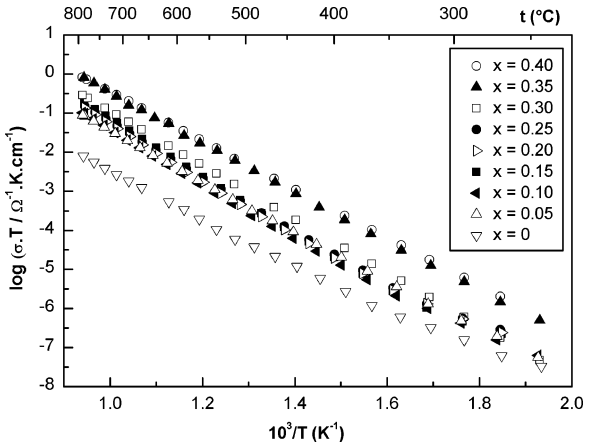

Figure 17. Conductivity data illustrating the influence of the Ge substitution rate on the transport properties of $Nd_4[Ga_{2(1-x)}Ge_{2x}O_{7+x}\square_{1-x}]O_2$ ($x \leq 0.4$) compounds (all densities ~98%).

The influence of the Ge substitution rate was investigated on a complete set of $Nd_4[Ga_{2(1-x)}Ge_{2x}O_{7+x}\square_{1-x}]O_2$ ($x \leq 0.4$) samples, all prepared by the sol gel method mentioned above, i.e., with densities ~98%. The corresponding Arrhenius plots are presented in Figure 17. They highlight the beneficial role of the Ge substitution for Ga (and of the concomitant filling of oxygen vacancies) on the anionic conductivity which increases rather regularly when x increases. This latter result contradicts our previous study[1] showing that the conductivity was going through a maximum for $x = 0.1$. Previous measurements were made with the use of samples prepared by solid state reaction, likely not very dense, and which therefore should have led to lower conductivities. That a higher conductivity was previously measured for $x = 0.1$ could well be due to some diffusion of the Pt paste in pores of this particular pellet, leading to a geometrical factor (thickness/area) smaller than that inferred from the actual dimensions of the pellet. In the present study, the highest conductivity at 800 °C, $\sigma = 10^{-3}$ S/cm, is obtained for $x = 0.4$. Figure 18 shows that E_a increases linearly up to $x = 0.2$ as a possible consequence of a more covalent framework when Ga^{3+} is replaced by Ge^{4+}. Its linear decrease when x is further increased could well be related with the 2D disorder which

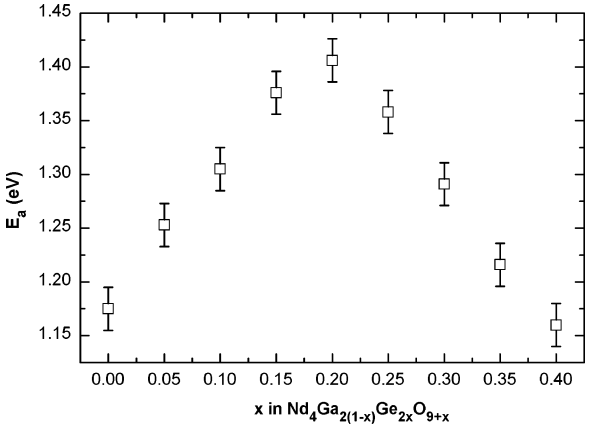

Figure 18. $Nd_4[Ga_{2(1-x)}Ge_{2x}O_{7+x}\square_{1-x}]O_2$ ($x \leq 0.4$) compounds: evolution of the activation energy vs x in the 400−800 °C range.

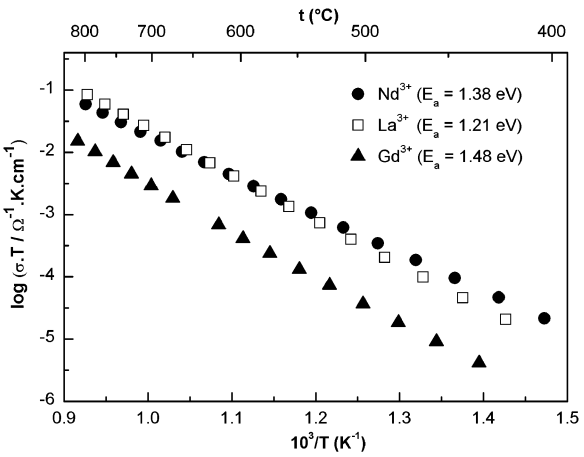

Figure 19. Conductivity data for $Ln_4[Ga_{1.6}Ge_{0.4}O_{7.2}\square_{0.8}]O_2$ compounds.

appears in the modulated structure for the largest x values.

For a fixed Ge content ($x = 0.2$) electrical measurements were also made in order to evaluate the role of the Ln^{3+} cation size on the ion conductivity and activation energy of $Ln_4[Ga_{1.6}Ge_{0.4}O_{7.2}\square_{0.8}]O_2$ compounds. La^{3+} (effective ionic radii in 6-fold coordination: $r_e^{(VI)} = 1.032$ Å[12]) and Gd^{3+} ($r_e^{(VI)} = 0.938$ Å) were chosen as they are, respectively, larger and smaller than Nd^{3+} ($r_e^{(VI)} = 0.983$ Å). The corresponding Arrhenius plots are displayed in Figure 19. It can be seen that the conductivities of La and Nd compounds between 400 and 800 °C are almost identical but significantly larger than that of the Gd counterpart. Concerning E_a there is a clear increase when r_e decreases, and this is likely a consequence of an increasing polarizing effect of the Ln^{3+} cation when its size decreases.

Finally, though La^{3+}, Nd^{3+}, Gd^{3+}, Ga^{3+}, and Ge^{4+} are not known to be sensitive either to reduction or oxidation, $Ln_4[Ga_{1.6}Ge_{0.4}O_{7.2}\square_{0.8}]O_2$ compounds (Ln = La, Nd, Gd) were subjected to conductivity measurements under two reduced oxygen partial pressures (10^{-5} and 10^{-20} atm). As expected, it was shown that, within experimental error, the conductivities are almost identical to those measured in air which indicates pure oxide-ion conduction in these materials.

4. Conclusion

The (Ln = La, Nd, Gd) compounds exhibit a Cuspidine-like structure up to $x = 0.4$. This higher limit in the substitution of Ge^{4+} for Ga^{3+} has been explained on the basis of structural considerations and by assuming that Ga^{3+} is much more propitious to 5-fold coordination than Ge^{4+}. From a SAED study it has been shown that for $x = 0.15$ a 1D modulation appears along the c_o axis of the structure. For larger Ge contents, besides modulation, a disorder is observed in the (b_o, c_o) plane. A simple model of 1D modulation has been proposed. Based on the possible distributions of both Ga,Ge and O,□ along the c_o axis, it appears as driven by composition only.

Thanks to a new regenerative sol−gel method, the title compounds have been prepared in the form of dense pellets allowing us to perform electrical measurements more reliable than those in a previous study.[1] It has been shown that when the density increases from 78 to 98% of the theoretical, the conductivity is multiplied by about two. For a fixed Ge content the conductivities of La and Nd compounds between 400 and 800 °C are almost identical but significantly larger than that of the Gd counterpart. In the present study, the highest conductivity at 800 °C, $\sigma = 10^{-3}$ S/cm, is obtained for $Nd_4[Ga_{1.2}Ge_{0.8}O_{7.4}\square_{0.6}]O_2$.

Acknowledgment. S.G. (Present address: Department of Physics, Southern University at Baton Rouge, Baton Rouge, LA 70813) gratefully acknowledges financial support of the "Région des Pays de la Loire" in the form of a postdoctoral fellowship for eleven months.

CM048910T

(12) Shannon, R. D. *Acta Crystallogr.* **1976**, *A32*, 751.